Minimum switching thruster control for spacecraft precision pointing

1

Mirko Leomanni, Andrea Garulli, *Senior Member, IEEE*,
Antonio Giannitrapani, *Member, IEEE*, Francesco Farina, *Student Member, IEEE*and Fabrizio Scortecci

Abstract

Maintaining the attitude of a spacecraft precisely aligned to a given orientation is crucial for commercial and scientific space missions. The problem becomes challenging when on/off thrusters are employed instead of momentum exchange devices due to, e.g., wheel failures or power limitations. In this case, the attitude control system must enforce an oscillating motion about the setpoint, so as to minimize the switching frequency of the actuators, while guaranteeing a predefined pointing accuracy and rejecting the external disturbances. This paper develops a three-axis attitude control scheme for this problem, accounting for the limitations imposed by the thruster technology. The proposed technique is able to track both the period and the phase of periodic oscillations along the rotational axes, which is instrumental to minimize the switching frequency in the presence of input coupling. Two simulation case studies of a geostationary mission and a low Earth orbit mission are reported, showing that the proposed controller can effectively deal with both constant and time-varying disturbance torques.

Index Terms

Minimum switching control, On/off thrusters, Attitude control, Optimal control.

I. INTRODUCTION

Spacecraft attitude control systems based on reaction thrusters have been widely used in the past (see e.g. [1], [2]) and are receiving renewed attention with the recent advances of micropropulsion technologies [3], [4], [5], [6]. The advent of electric micropropulsion [7], [8], providing a much higher fuel

M. Leomanni, A. Garulli, A. Giannitrapani and F. Farina are with the Dipartimento di Ingegneria dell'Informazaione e Scienze Matematiche, Università di Siena, Siena, Italy. F. Scortecci is with Aerospazio Tecnologie s.r.l., Rapolano Terme (Siena), Italy. Email: {leomanni,garulli,giannitrapani,farina}@diism.unisi.it,fscortecci@aerospazio.com.

efficiency with respect to traditional cold-gas systems, further motivates the study of attitude regulation schemes involving reaction thrusters. In fact, this technological solution enables the development of all-electric spacecraft which exploit the same propellant type for both orbit control and precise attitude regulation, thus reducing costs and providing an effective complement to momentum exchange devices [9], [10]. On the other hand, these engines present some severe restrictions, the most important one concerning the fact that they are usually operated in on/off mode, which clearly limits the control authority. Moreover, the thruster switching frequency can have a significant impact on the performance and the lifetime of this type of actuators.

The use of on/off thrusters for spacecraft precision pointing calls for a switching controller delivering some kind of pulse modulation, in order to reject the external disturbances and to comply with the minimum firing time of the engines [11], [12], [13]. To achieve the best efficiency, the minimization of both the fuel consumption and the switching frequency of the actuators must be pursued. A common approach is to convert the control input provided by a continuous regulator into discrete pulses, by using pulse-width or pulse-width-pulse-frequency modulation techniques, see e.g. [14], [15], [16]. These methods hold significant advantages over conventional bang-bang control strategies, including a reduced thruster activity and a near-linear duty cycle, but require a time-consuming trial-and-error procedure to tune the modulator parameters, as outlined in [17], [18]. Another major drawback of these control techniques is that they do not allow the pointing accuracy requirements to be enforced directly as state constraints in the control problem.

A more general approach consists in the formulation of an optimal control problem, in which the on/off characteristics of the thrusters are explicitly taken into account, see e.g. [19], [20], [21]. However, very few contributions have addressed explicitly the minimization of the switching frequency. Until recently, results have been confined to the single-axis attitude control problem, with the error dynamics approximated by a double integrator model [22], [23]. In fact, the multivariable problem becomes very challenging when the control design cannot be decoupled along the principal axes of inertia of the spacecraft, due to the chosen thruster configuration. In [10], a model predictive control (MPC) scheme has been proposed for the thee-axis case. This method involves a high computational burden, which may not fit the processing power available onboard a spacecraft. In [24], [25], a periodic suboptimal solution to the minimum switching control problem has been derived for systems of double integrators perturbed by a constant disturbance.

By building on these preliminary results, this paper develops a high precision, three-axis attitude control scheme for spacecraft with on/off thrusters. As a first step in the design, the minimum fuel/switching control problem introduced in [24] is reformulated by including constraints on both the attitude error and its derivative. Two solutions to this problem are derived, providing reference trajectories to the attitude

regulation system. Then, an adaptive feedback control scheme is proposed, which extends the applicability of the control law derived in [25] to the case of time varying disturbances, while accounting for restrictions on the minimum duration of a thruster firing. The performance of this approach is investigated for geostationary (GEO) and low Earth orbit (LEO) missions. Simulations based on the full nonlinear attitude dynamic model show that the controller is able to meet the pointing accuracy requirements, in the presence of constant or slowly time-varying disturbance torques.

The paper is organized as follows. In Section II, the attitude dynamic model is introduced, along with the attitude control requirements. In Section III, the optimal attitude control problem is formulated and the reference trajectory to be tracked by the control system is derived. In Section IV, the thruster control scheme under consideration is presented. The performance of the proposed approach is evaluated through numerical simulations of a GEO mission and a LEO mission in Section V, while some concluding remarks are given in Section VI.

II. SPACECRAFT PRECISION POINTING

In this section, the small angle approximation of the attitude error dynamics is presented, and the attitude control requirements are discussed, for spacecraft precision pointing with on/off thrusters.

A. Notation

The orientation of a reference frame B with respect to a reference frame A is represented by the quaternion $q_{AB} = [\rho_{AB}, \vec{q}_{AB}^T]^T$, where ρ_{AB} and \vec{q}_{AB} are the scalar part and the vector part of the quaternion. The quaternion multiplication $q_{AC} = q_{BC} \circ q_{AB}$ is defined by

$$q_{AC} = \begin{bmatrix} \rho_{BC}\rho_{AB} - \vec{q}_{BC}^T \vec{q}_{AB} \\ \rho_{BC}\vec{q}_{AB} + \rho_{AB}\vec{q}_{BC} - \vec{q}_{BC} \times \vec{q}_{AB} \end{bmatrix}, \tag{1}$$

where \times denote the cross product operation and q_{AC} , q_{BC} represent the orientation of frame C with respect to frames A and B, respectively.

The skew-symmetric matrix constructed from a vector ω is denoted by ω^{\times} . The rest of the notation is standard: u_j indicates the j-th entry of vector u, $\|\cdot\|_p$ denotes the p-norm of vectors and matrices and $\operatorname{sgn}(\cdot)$ denotes the signum function, where it is assumed that $\operatorname{sgn}(0) = 1$.

B. Attitude error dynamics

The attitude of the spacecraft is described as the orientation of a reference frame centered at center of mass and aligned with the principal axes of inertia of the body, which is termed as the body frame, with respect to the Earth centered inertial frame. Let the orientation of the body frame with respect to

the inertial frame be denoted by the four-dimensional quaternion q_{IB} , and the angular rate of the body frame with respect to inertial frame, expressed in the body frame, be denoted by the three-dimensional vector ω_B . The kinematics of the attitude quaternion are given by

$$\dot{q}_{IB} = \frac{1}{2} \begin{bmatrix} 0 \\ \omega_B \end{bmatrix} \circ q_{IB}. \tag{2}$$

Under the rigid body assumption, the angular rate dynamics are given by

$$\dot{\omega}_B = I_M^{-1} \left(\tau_d + \tau_u - \omega_B^{\times} I_M \, \omega_B \right). \tag{3}$$

where I_M is the spacecraft inertia matrix and

$$\tau = \tau_d + \tau_u \tag{4}$$

denotes the torque acting on the system, including a disturbance torque τ_d and a control torque τ_u . For spacecraft equipped with on/off thrusters, the control torque τ_u can only take discrete values. Specifically, when a minimal set of thruster is employed, the control torque can be expressed as

$$\tau_u = M\mu,\tag{5}$$

where $\mu \in \{0,1\}^6$ represents the on/off thruster command, and the matrix M expresses the linear mapping from the thruster command to the control torque. For the common case in which the thruster configuration is symmetric, so that torques of opposite direction are produced with respect to the rotational axes, one has M = [-B, B] and (5) can be rewritten as

$$\tau_u = B\,\tilde{\mu},\tag{6}$$

where $\tilde{\mu} \in \{-1, 0, 1\}^3$.

The desired attitude and rotation rate are specified by the orientation q_{IR} of a target reference frame with respect to the inertial frame and by the angular velocity ω_R of the target frame with respect to the inertial frame, expressed in the target frame. Let q_{RI} denote the inverse rotation of q_{IR} . Using quaternion algebra, the attitude error q_{RB} , which indicates the orientation of the body frame relative to the target frame, can be expressed as $q_{RB} = q_{IB} \circ q_{RI}$. If the attitude error is small, it can be approximated by the three-dimensional rotation vector $\delta\theta$, which is obtained from the vector part \vec{q}_{RB} of the attitude error quaternion as

$$\delta\theta = 2\vec{q}_{RB}.\tag{7}$$

Now, let us define

$$\delta\omega = \omega_B - \omega_R. \tag{8}$$

For small $\delta\theta$ and $\delta\omega$, the kinematics of the attitude error (7) and the dynamics of the angular velocity error (8) can be approximated by a linearized model. The linearized kinematic model is given by the Bortz equation [26]

$$\delta\dot{\theta} = \delta\omega - \omega_R^{\times}\delta\theta,\tag{9}$$

where the term $\omega_R^{\times}\delta\theta$ accounts for the fact that ω_B and ω_R in (8) are expressed in two different coordinate frames. Concerning the dynamic model, by differentiating (8) with respect to time and exploiting (3), one gets

$$\delta \dot{\omega} = I_M^{-1} \tau - I_M^{-1} (\omega_R + \delta \omega)^{\times} I_M (\omega_R + \delta \omega) - \dot{\omega}_R. \tag{10}$$

In most practical applications, the target frame is either spinning at a constant angular velocity or inertially fixed. In the first case, the linearized dynamic model is found by enforcing $\dot{\omega}_R = 0$ in (10) and linearizing the resulting expression about $\delta\omega = 0$, thus yielding

$$\delta\dot{\omega} = A\delta\omega + I_M^{-1}\tau,\tag{11}$$

where $I_M = \operatorname{diag}(\iota_1, \, \iota_2, \, \iota_3),$

$$A = \begin{bmatrix} 0 & \frac{\iota_2 - \iota_3}{\iota_1} \,\omega_3 & \frac{\iota_2 - \iota_3}{\iota_1} \,\omega_2 \\ \frac{\iota_3 - \iota_1}{\iota_2} \,\omega_3 & 0 & \frac{\iota_3 - \iota_1}{\iota_2} \,\omega_1 \\ \frac{\iota_1 - \iota_2}{\iota_3} \,\omega_2 & \frac{\iota_1 - \iota_2}{\iota_3} \,\omega_1 & 0 \end{bmatrix}, \tag{12}$$

 ι_j denotes the principal moments of inertia and $\omega_R = [\omega_1, \omega_2, \omega_3]^T$. For the case in which the desired attitude is inertially fixed, one has $\omega_R = 0$ in (9) and (11)-(12). Hence, the error dynamics take on the form of the double integrator system

$$\delta \ddot{\theta} = I_M^{-1} \tau. \tag{13}$$

As long as precise attitude control of Earth-pointing spacecraft is concerned, gyroscopic inter-axis coupling is negligible [23] and the dynamics (9),(11) are well approximated by system (13). By applying the coordinate transformation

$$x = G^{-1}B^{-1}I_M \,\delta\theta,\tag{14}$$

$$u = G^{-1}\,\tilde{\mu},\tag{15}$$

$$k = G^{-1} \rho, \tag{16}$$

where $\varrho=B^{-1}\, au_d$ and $G=\mathrm{diag}(\mathrm{sgn}(\varrho)),$ system (13) can be cast into the equivalent form

$$\ddot{x} = u + k,\tag{17}$$

with $k \ge 0$. In this paper, model (17) will be used to design the control scheme to be applied to system (2)-(6) for disturbance rejection and attitude regulation.

C. Attitude control requirements

Due to the presence of on/off input restrictions and of persistent disturbances affecting the attitude dynamics (2)-(6), the system cannot be regulated exactly to the origin with a finite input switching frequency. Therefore, the attitude errors (7) and rate errors (9) must be controlled within a predefined accuracy. Formally, this amounts to ensure that

$$||W_p \,\delta\theta(t)||_{\infty} \le 1,$$

$$||W_r \,\delta\dot{\theta}(t)||_{\infty} \le 1,$$
(18)

where the weighting matrices W_p and W_r are usually diagonal. For system (17), according to the transformation (14)-(16), the pointing accuracy requirements (18) become

$$||C x(t)||_{\infty} \le 1,$$

 $||D \dot{x}(t)||_{\infty} \le 1,$ (19)

where

$$C = W_p I_M^{-1} B,$$

$$D = W_r I_M^{-1} B.$$
(20)

Notice that G does not appear in the right hand side of (20), as it would not change constraints (19). Moreover, the dynamics of system (17) are decoupled, but the state constraints (19) are coupled if the input matrix B is not diagonal. This occurs frequently in applications, e.g., whenever non-orthogonal thruster configurations are adopted, in order to meet constraints coming from the spacecraft layout or to maximize the efficiency of the propulsion system.

Besides guaranteeing that (19) holds, the control system is required to minimize both the fuel consumption and the switching frequency of the thrusters. In fact, the former is a limiting factor for the lifetime and the capabilities of the spacecraft, while the latter is proportional to the number of thruster valve activations and hence to the electrical power consumption and the wear of the engines. This problem will be addressed in detail throughout the rest of the paper.

III. REFERENCE TRAJECTORY OPTIMIZATION

In the section, the optimal attitude control problem is formulated and two suboptimal solutions are derived, providing reference trajectories to be tracked by the thruster controller. We will make the simplifying assumption that k in (17) is constant, since in the considered application the disturbance variation is usually much slower than the attitude error dynamics.

The average fuel consumption is defined as

$$J_f(u) = \lim_{T \to \infty} \frac{1}{T} \int_0^T ||u(t)||_1 dt.$$
 (21)

Notice that any input sequence for which $J_f(u) < ||k||_1$ cannot satisfy both constraints (19) indefinitely. In addition, it can be shown that any sequence of the form

$$u_j(t) \in \{-1, 0\}, \quad j = 1, 2, 3,$$
 (22)

guaranteeing that (19) hold, is such that $J_f(u) = ||k||_1$, and therefore it is fuel-optimal [24]. Among all the fuel-optimal input sequences, we aim at finding the one which minimizes the thruster switching frequency.

The switching frequency of a single thruster can be expressed as the average number of input transitions per time unit, commanded by the control system. This is given by

$$J_s(u_j) = \lim_{T \to \infty} \frac{1}{T} \int_0^T |\dot{u}_j(t)| dt.$$
 (23)

Since we are interested in reducing as much as possible the fuel consumption and the number of input transitions per actuator, while satisfying the state constraints, the optimal control problem can be formulated as

$$\min_{u} \max_{j} J_{s}(u_{j})$$
s.t. (17), (19), (22).

Hereafter, the single-axis solution to problem (24) is briefly reviewed and suitably extended to the multivariable case. We will restrict our attention to the case k > 0, since for k = 0 system (17) can be steered to the origin in finite time by using well-known results from the literature [27] (notice that this does not hold when restrictions on the duration of thruster firings are taken into account; this case will be addressed in Section IV-B).

A. Single-axis solution

Consider a single-axis double integrator $(x \in \mathbb{R})$. In this case, the solution to problem (24) is known since long time [28], and corresponds to the limit cycle oscillation $\psi^U \cup \psi^L$ depicted in the phase plane in Fig. 1, where

$$\psi_L = \{(x, \dot{x}) : x - \frac{1}{2k} \dot{x}^2 = -a, \quad -a \le x < a(1 - 2k)\},\tag{25}$$

$$\psi_U = \{(x, \dot{x}): \ x - \frac{1}{2(k-1)}\dot{x}^2 = a, \ a(1-2k) \le x \le a\},\tag{26}$$

 $u^* = -1$ when $(x, \dot{x}) \in \psi^U$, $u^* = 0$ when $(x, \dot{x}) \in \psi^L$, and a denotes the oscillation amplitude. When constraints on the attitude error rate are not enforced (i.e. D = 0 in (19)), one has trivially that a = 1/C. In the presence of both attitude error and attitude error rate constraints, the amplitude is given by

$$a = \min\left(\frac{1}{C}, \frac{1}{64\gamma D^2}\right),\tag{27}$$

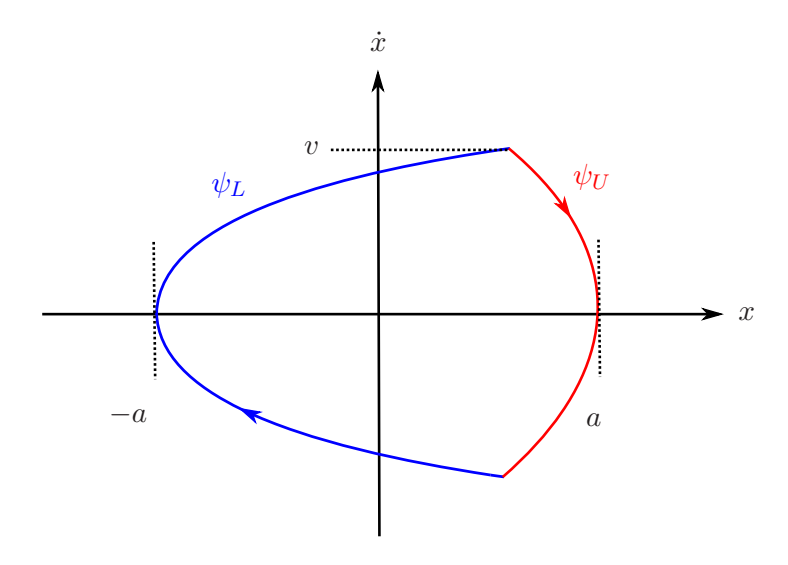


Fig. 1. Limit cycle obtained by solving problem (24): single-axis case.

where $\gamma = k(1-k)/16$, the peak velocity along the limit cycle being $v = 8\sqrt{\gamma a}$. Notice that the period of the oscillation is $p = \sqrt{a/\gamma}$ and the resulting input switching frequency is $J_s(u^*) = 2/p$. To verify that the provided minimum switching solution is also a fuel optimal solution, observe that the time spent along the branch ψ_U of the limit cycle is equal to kp. Then, it can be easily shown that $J_f(u^*) = k$.

B. Multi-axis solution

Except for the trivial case in which C and D are diagonal, the multivariable problem (24) is hard to solve if all feasible input signals u(t) are considered. Therefore, by building on the optimal solution of the single-axis problem, we restrict our attention to the class of input sequences which generate periodic trajectories of the form depicted in Fig. 1, for each axis. This corresponds to parameterizing the trajectory of the j-th double integrator as

$$x_{j}(t) = p_{j}^{2} \gamma_{j} f_{j}(\lambda_{j}),$$

$$\lambda_{j} = \operatorname{mod}(t/p_{j} + \phi_{j}, 1),$$
(28)

where $\gamma_j = k_j (1 - k_j)/16$, p_j is the period, $\phi_j \in [0, 1)$ is the phase, mod(a, b) indicates the remainder of a/b, and $f_j(\lambda_j) \in [-1, 1]$ is defined as

$$f_{j}(\lambda_{j}) = \begin{cases} 1 - \frac{8}{k_{j}} (\lambda_{j} - \frac{k_{j}}{2})^{2} & \text{if } 0 \leq \lambda_{j} \leq k_{j} \\ -1 - \frac{8}{k_{j} - 1} (\lambda_{j} - \frac{k_{j} + 1}{2})^{2} & \text{if } k_{j} < \lambda_{j} < 1. \end{cases}$$
(29)

The inputs $u_j(t)$ giving rise to $x_j(t)$ of the form (28) are pulse-width modulated signals with period p_j and duty cycle k_j , and can be expressed as

$$u_j(t) = \begin{cases} -1 & \text{if } 0 \le \lambda_j \le k_j \\ 0 & \text{if } k_j < \lambda_j < 1. \end{cases}$$
 (30)

The input signals u_j in (30) are fuel-optimal, because $J_f(u) = ||k||_1$. Being these signals double-switch periodic, one has $J_s(u_j) = 2/p_j$. Moreover, (19) is equivalent to

$$\max_{i} \max_{t} \left| \sum_{j=1}^{3} C_{ij} x_{j}(t) \right| \leq 1,$$

$$\max_{i} \max_{t} \left| \sum_{j=1}^{3} D_{ij} \dot{x}_{j}(t) \right| \leq 1,$$
(31)

where the coefficients C_{ij} and D_{ij} are the entries of C and D. By enforcing (28) and replacing (19) by (31), problem (24) becomes

$$\min_{p,\phi} \max_{j} 2/p_{j}$$
s.t. (28), (31)
$$0 \le \phi_{j} < 1$$

$$p_{j} > 0, \quad j = 1, 2, 3,$$
(32)

where $p = [p_1, p_2, p_3]^T$ and $\phi = [\phi_1, \phi_2, \phi_3]^T$.

This way, the dynamic optimization problem (24) has been converted into a static optimization problem, where the decision variables are p and ϕ . Note, however, that the problem is still hard to solve, being non-convex in these decision variables. Consequently, some simplifying assumptions will be made in order to derive an upper bound to the solution of (32). Let us observe that by (28)

$$\max_{i} \max_{t} \left| \sum_{j=1}^{3} C_{ij} x_{j}(t) \right| \leq \max_{i} \sum_{j=1}^{3} |C_{ij}| a_{j},$$

$$\max_{i} \max_{t} \left| \sum_{j=1}^{3} D_{ij} \dot{x}_{j}(t) \right| \leq \max_{i} \sum_{j=1}^{3} |D_{ij}| v_{j},$$
(33)

where

$$a_{j} = \max_{t} x(t) = p_{j}^{2} \gamma_{j},$$

$$v_{j} = \max_{t} \dot{x}(t) = 8\sqrt{\gamma_{j} a_{j}}.$$
(34)

Hence, (31) can be guaranteed by imposing

$$\|\overline{C} a\|_{\infty} \le 1,$$

$$\|\overline{D} v\|_{\infty} < 1,$$
(35)

where $a = [a_1, a_2, a_3]^T$, $v = [v_1, v_2, v_3]^T$ and \overline{C} , \overline{D} are the matrices whose entries are $|C_{ij}|$ and $|D_{ij}|$. By replacing (31) with (35) and exploiting (34), problem (32) boils down to

$$\min_{a} \max_{j} 2\sqrt{\frac{\gamma_{j}}{a_{j}}}$$
s.t. (35)
$$a_{j} > 0, \quad j = 1, 2, 3.$$
(36)

By (33), the solution of (36) is an upper bound to that of (32). It turns out that problem (36) can be solved analytically, as stated by the following theorem.

Theorem 1: A global minimum of problem (36) is attained at

$$a^* = \frac{1}{\max\{\|Q\|_{\infty}, \|S\|_{\infty}^2\}} \Gamma \mathbb{1}, \tag{37}$$

where $\Gamma = \operatorname{diag}(\gamma_1, \gamma_2, \gamma_3)$, $Q = \overline{C}\Gamma$, $S = 8\overline{D}\Gamma$, and $\mathbb{1} = [1, 1, 1]^T$.

Proof: The proof is reported in the Appendix.

Since by (37) all the entries of $\Gamma^{-1}a^*$ are equal, it follows from the relationship $p_j = \sqrt{a_j/\gamma_j}$ that the trajectories corresponding to the solution of problem (36) have the same period

$$p_1 = p_2 = p_3 = \max\{\sqrt{\|Q\|_{\infty}}, \|S\|_{\infty}\}^{-1}.$$
 (38)

Notice that the period (38) depends on the value of k.

A less conservative relaxation of problem (32) can be found by exploiting the relative phases ϕ_j in (28). In order to make the problem computationally tractable, we enforce directly the property $p_1 = p_2 = p_3$ in (32). This leads to the new relaxed problem

$$\min_{p,\phi} 2/p_1
s.t. (28), (31)
\phi_1 = 0,
0 \le \phi_j < 1, j = 2, 3,
p_1 = p_2 = p_3 > 0,$$
(39)

where $\phi_1 = 0$ has been set without loss of generality, since shifting all the phases by the same quantity does not alter the optimal solution of (39). The following result holds.

Theorem 2: A global minimum of problem (39) is attained at

$$\phi^* = \underset{\phi}{\operatorname{argmin}} \max \{ \sqrt{\sigma(\phi)}, \, \eta(\phi) \},$$

$$p_1^* = p_2^* = p_3^* = \max \{ \sqrt{\sigma(\phi^*)}, \eta(\phi^*) \}^{-1},$$
(40)

where

$$\sigma(\phi) = \max_{i} \max_{0 \le t \le 1} \left| \sum_{j=1}^{3} C_{ij} \gamma_{j} f_{j}(t + \phi_{j}) \right|,$$

$$\eta(\phi) = \max_{i} \max_{0 \le t \le 1} \left| \sum_{j=1}^{3} D_{ij} \gamma_{j} \dot{f}_{j}(t + \phi_{j}) \right|.$$

$$(41)$$

Proof: The proof is reported in the Appendix.

Due to (33) and (38), the solution of problem (39) is a lower bound to that of (36), and an upper bound to that of (32). According to (30), the resulting optimal input signals u_j^* are pulse-width modulated with period $p_j^* = p_1^*$ and phases $\phi_1^* = 0$ and ϕ_j^* for j = 2, 3. Being $\sigma(\phi)$ and $\eta(\phi)$ non convex functions, the global minimizer (40) can be found by numeric search over the free phases ϕ_2 and ϕ_3 , as illustrated by the following example.

Example 1. Let

$$C = \begin{bmatrix} 0 & 0 & -0.053 \\ -0.055 & 0.055 & 0 \\ -0.055 & 0.055 & 0.055 \end{bmatrix}, \tag{42}$$

D=0 and $k=[0.2,\,0.3,\,0.6]^T$. Theorem 1 gives $a^*=[4.73,6.21,7.10]^T$, which corresponds to the period $p_1^*=p_2^*=p_3^*=22.22$ and the optimal cost $J_s(u_j^*)=0.090$. In order to compute the solution provided by Theorem 2, one has to search the 2-dimensional parameter space ϕ_2,ϕ_3 for a global minimizer of $\sigma(\phi)$. This gives $\phi_2^*=0.90,\,\phi_3^*=0.07$ and $p_1^*=p_2^*=p_3^*=35.60$, corresponding to the optimal cost $J_s(u_j^*)=0.056$. Notice from Fig. 2 that $\sigma(\phi)$ is a non-convex function of the decision variables ϕ with multiple local minima. As expected, Theorem 2 requires a lower switching frequency, while the average fuel consumption is the same for both solutions, by construction. In particular, the optimal cost of (39) is lower than the optimal cost of (36) by approximately 39%. The three-dimensional plot of the trajectories $x_1(t),\,x_2(t)$ and $x_3(t)$ is reported in Fig. 3, where it can be seen that the control accuracy requirements (represented by the 3-dimensional parallelotope) are satisfied.

IV. THRUSTER CONTROL

In this section the problem of tracking the reference trajectories corresponding to the periodic solutions derived in Section III is addressed. First, the control law recently developed in [25], for the case of constant disturbances, is briefly recalled. Then, an adaptive control scheme is proposed, which accounts for the minimum firing duration imposed by the thruster technology and the presence of time-varying disturbances.

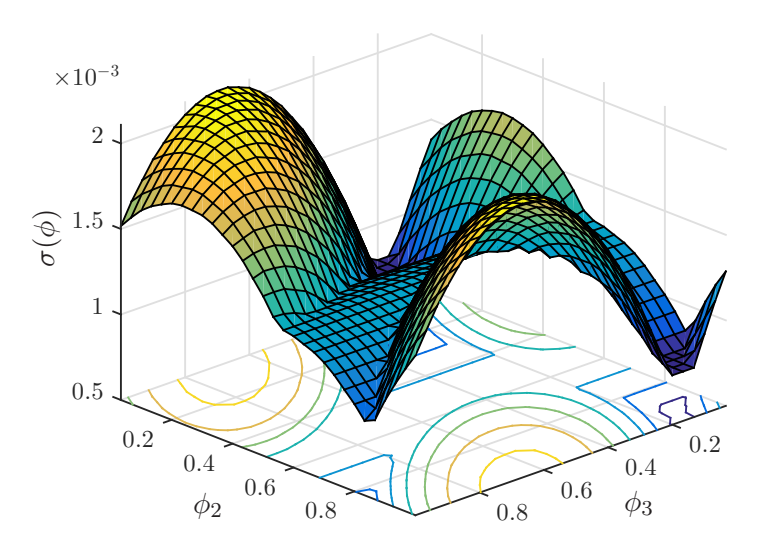


Fig. 2. An example of function $\sigma(\phi)$ in (41).

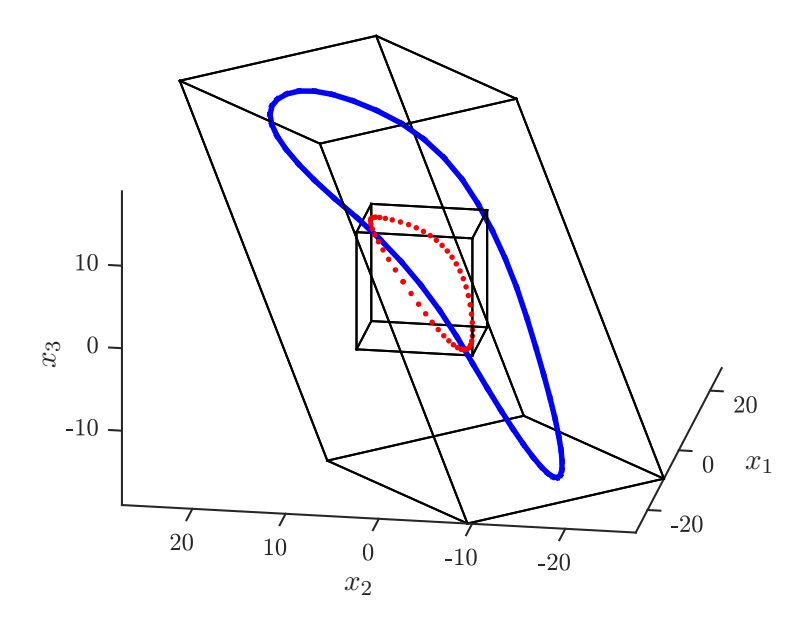


Fig. 3. Trajectories resulting from the solution to (36) (dotted) and (39) (solid), together with constraints $||Cx||_{\infty} \le 1$ (outer parallelotope) and $|x_i| \le a_i^*$ (inner box).

A. Reference trajectory tracking

Since in system (17) the three double integrators are decoupled, three single-axis feedback control laws (one per input channel), can be used to track the reference trajectories provided by Theorems 1 and 2. This corresponds to steering system (17) to a trajectory of the form (28) with a prescribed period

(Theorem 1), or both a prescribed period and phase (Theorem 2), from any initial condition. For ease of exposition, in the following the subscript j is dropped from the notation (i.e., it is left intended that $x = x_j$, $a = a_j$, $p = p_j$, $\phi = \phi_j$, $k = k_j$, unless otherwise indicated).

Let us start by showing how to steer system (17) to a trajectory of the form (28) with given period p, under the assumption of a constant disturbance k. The following control law, termed MS_I, can be adopted

$$\mathbf{MS}_{\mathbf{I}}(a): \ u(t) = \begin{cases} -1 \text{ if } \ s(x, \dot{x}; k) \ge a \\ 0 \text{ if } \ s(x, \dot{x}; k) \le -a \\ u_p \text{ otherwise,} \end{cases}$$

$$(43)$$

where $u_p=-1$ if $s(x,\dot{x};k)\geq a$ occurred more recently than $s(x,\dot{x};k)\leq -a$, $u_p=0$ otherwise. Moreover,

$$s(x, \dot{x}; k) = \begin{cases} x - \frac{1}{2(k-1)} \dot{x}^2 & \text{if } \dot{x} \ge 0\\ x - \frac{1}{2k} \dot{x}^2 & \text{if } \dot{x} < 0 \end{cases}$$
(44)

is the classical fuel-optimal switching function for the double integrator subject to a constant load k (see e.g. [29]). Notice that (43)-(44) describe a relay feedback system with hysteresis defined by a.

The switching curves $s(x,\dot{x};k)=a$ and $s(x,\dot{x};k)=-a$ are reported in the phase plane in Fig. 4, together with an example of a controlled trajectory (dotted). It is apparent that, by applying the control law MS_I to each axis of the perturbed double integrator (17), a trajectory of the form (28) with period $p=\sqrt{a/\gamma}$ is reached in finite time, using only one switching per input channel, from any initial condition. Therefore, the reference trajectory specified by Theorem 1 can be tracked by using the control law MS_I(a^*), with a^* given by (37).

In order to achieve the solution provided by Theorem 2, a prescribed phase must be tracked in addition to the period. In [25], a control law has been introduced to this purpose, which exploits a time-varying hysteresis defined by two parameters a^U and a^L . More specifically, the control law (43) is modified as

$$\mathbf{MS}_{\Pi}(p,\phi): \ u(t) = \begin{cases} -1 & \text{if} \quad s(x,\dot{x};k) \ge a^{U}(t;p,\phi) \\ 0 & \text{if} \quad s(x,\dot{x};k) \le -a^{L}(t;p,\phi) \\ u_{p} & \text{otherwise,} \end{cases}$$

$$(45)$$

where $u_p=-1$ if $s(x,\dot{x};k)\geq a^U$ occurred more recently than $s(x,\dot{x};k)\leq -a^L$, $u_p=0$ otherwise, and $a^L+a^U>0$. The idea is to update the offset of a switching curve whenever the opposite curve is reached, so as to steer the system to a periodic solution with given period p and phase ϕ . By assuming without loss of generality that the curve which is hit first is $s(x,\dot{x};k)=a^U$ at time z_1 , this results in piece-wise constant parameters

$$a^{L}(t; p, \phi) = h_{2m-1} \text{ for } t \in [z_{2m-1}, z_{2m+1}),$$

 $a^{U}(t; p, \phi) = h_{2m} \text{ for } t \in [z_{2m}, z_{2m+2}),$

$$(46)$$

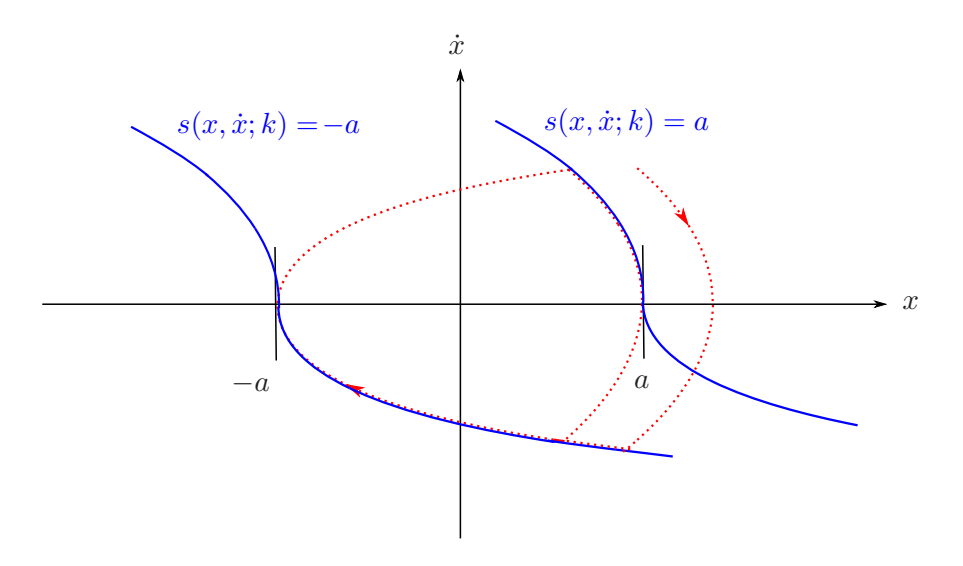


Fig. 4. Switching curves (solid) and example of a trajectory (dotted) from the application of the MS_I control law.

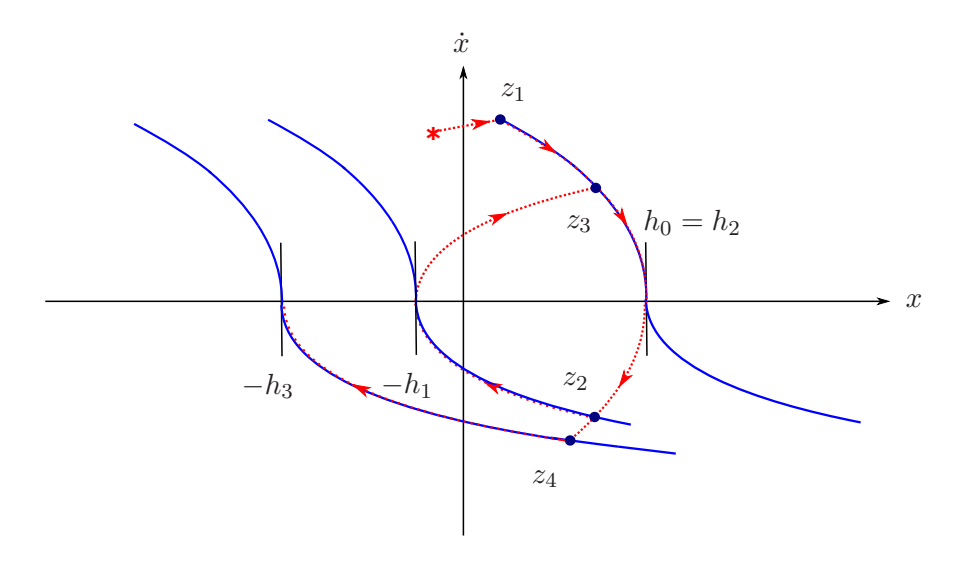


Fig. 5. Switching curves (solid) and example of a trajectory (dotted) from the application of the MS_{II} control law.

where the sequence $\{z_l\}$ denotes the time instants at which the state trajectory reaches a switching curve (an example is shown in Fig. 5). The sequence $\{h_l\}$ defining these parameters is given by

$$h_0 = p^2 \gamma, \tag{47}$$

$$h_l = p^2 \gamma \left(1 + 4\Delta \phi_l + 2\Delta \phi_l^2 \right), \tag{48}$$

where

$$\Delta \phi_l = \text{mod}\left(\frac{\bar{z}_{l+2} - \hat{z}_{l+2}}{p} + \frac{1}{2}, 1\right) - \frac{1}{2},\tag{49}$$

$$\hat{z}_{l+2} = z_l + \frac{|\dot{x}(z_l)|}{q(z_l)} + \frac{q(z_l)}{2}p + \frac{\sqrt{2}}{4}\sqrt{p^2 + \frac{h_{l-1}}{\gamma}},\tag{50}$$

 $q(z_l) = |u(z_l) + d|$, and $\{\bar{z}_l\}$ is defined according to

$$\bar{z}_{2m-1} = -\phi p,
\bar{z}_{2m} = (k - \phi) p.$$
(51)

It is shown in [25] that, by applying to each rotational axis the control law $MS_{II}(p^*, \phi^*)$, with p^* and ϕ^* given by (40), system (17) is steered in finite time to the reference trajectory (28) provided by Theorem 2. Moreover, only three switchings of the control input are required to reach this trajectory from any initial condition.

Example 2. Consider the problem of tracking the reference trajectory specified by Theorem 2 in Example 1 (i.e. the blue, solid trajectory in Fig. 3). For each input channel of system (17), the control law MS_{II} is implemented through the event-based switching logic depicted in Fig. 6. The initial conditions for the simulation are set to $x(t_0) = [10, 25, -10]^T$ and $\dot{x}(t_0) = [3, 2, -4]^T$. The trajectory of the closed-loop system is reported in Fig. 7. It can be clearly seen that, after a finite transient, the system trajectory converges to the reference limit cycle (marked). The corresponding control inputs are reported in Fig. 8. As expected, the desired duty cycle is attained from the fourth input transition onwards, for each input channel.

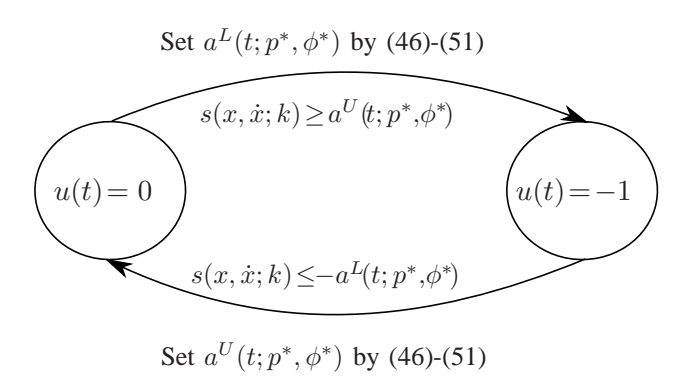


Fig. 6. Event-based switching logic.

B. Firing duration restrictions

If one or more elements k_j of the the disturbance vector k in (17) are close to zero, the firing time required by the MS_I and MS_{II} schemes may not be compatible with the minimum pulse duration Δt_m

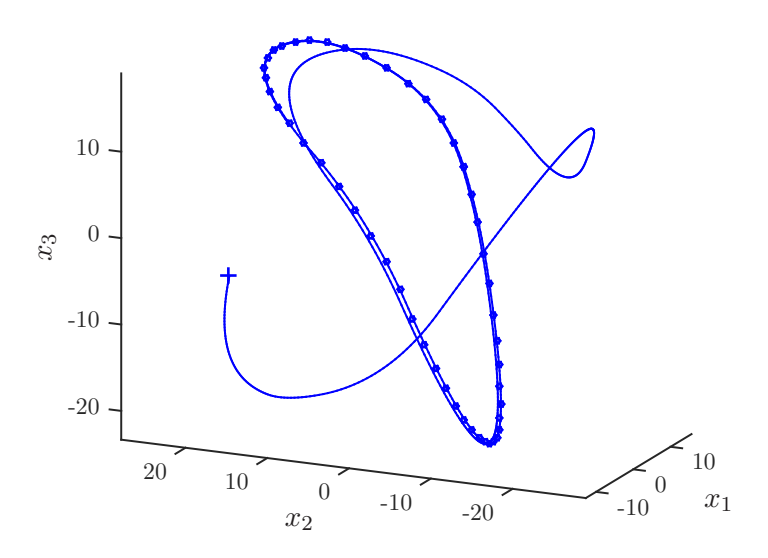


Fig. 7. Closed-loop trajectory (solid) and reference limit cycle (marked).

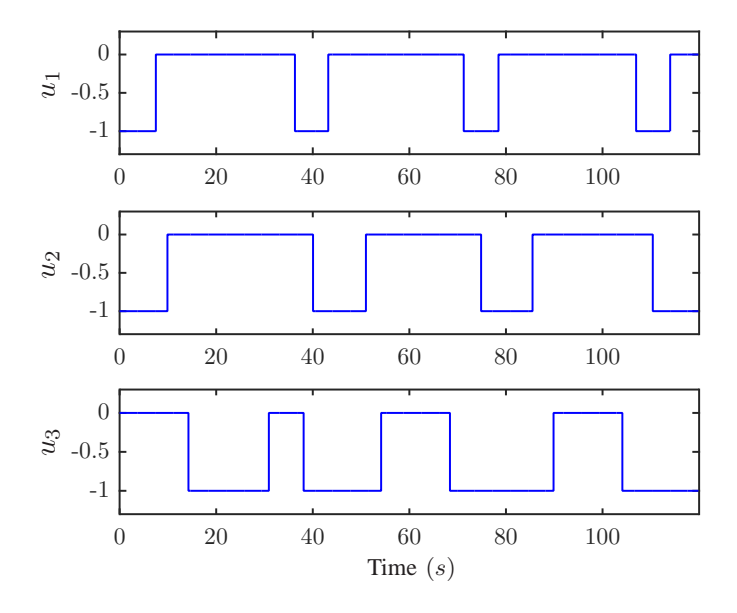


Fig. 8. Control inputs.

imposed by the thruster technology. This must be taken into account for a reliable implementation of the control system. In particular, in order to ensure the feasibility of the reference trajectory provided by Theorem 2, one must have $k_j p_j^* \geq \Delta t_m \ \forall j$, where $k_j p_j^*$ is the required duration of the j-th thruster firing according to (28)-(30). Conversely, when $k_j p_j^* < \Delta t_m$ for some j, there is no input signal $u_j \in \{-1,0\}$

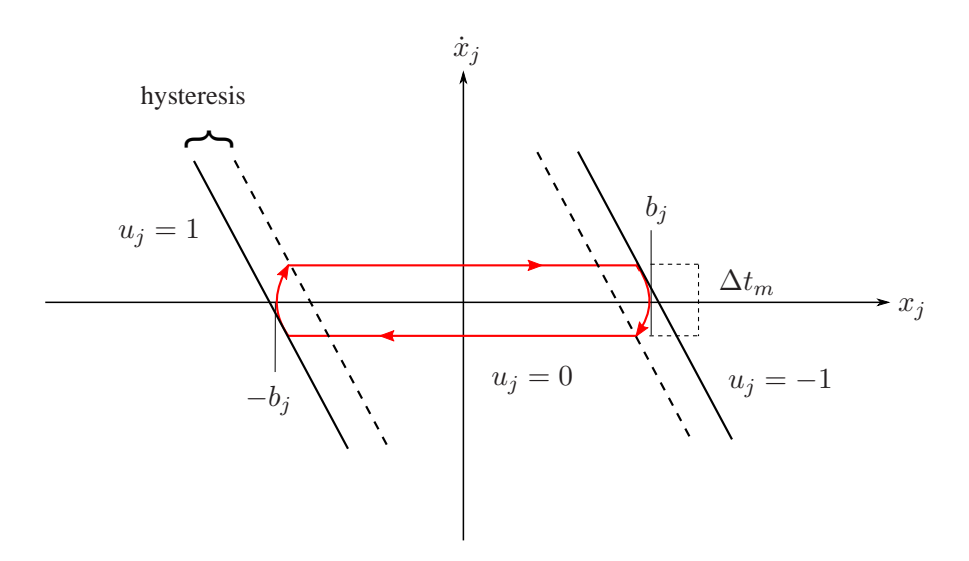


Fig. 9. Oscillation resulting from the application of the $MS_0(b_j)$ scheme, with $k_j = 0$.

which guarantees that (19) holds, i.e. problem (24) does not admit any feasible solution of the considered form. To circumvent this issue, one possibility is to enforce an oscillating motion in which $u_j = -1$ and $u_j = 1$ are applied for the minimum possible firing interval Δt_m , so as to keep the attitude error within a bound b_j , i.e. $|x_j| \leq b_j$. A standard control scheme based on linear switching functions with deadzone and hysteresis (Schmitt trigger), which is denoted by $MS_0(b_j)$, can be adopted to this purpose, see e.g. [30]. The resulting trajectory is reported in the phase plane in Fig. 9, for the case $k_j = 0$. One can verify that both the fuel consumption and the input switching frequency required by such trajectory are proportional to $1/b_j$. Hence, the objective of the minimum switching problem becomes to optimize over the parameters b_j , while guaranteeing that constraints (19) are satisfied. This can be done by applying the same relaxation leading to problem (36), which amounts to solve the static optimization problem

$$\min_{b} \max_{j} \frac{1}{b_{j}}$$
s.t. $\|\overline{C}b\|_{\infty} \le 1$

$$b_{j} > 0, \quad j = 1, 2, 3.$$

$$(52)$$

By using the same reasoning as in Theorem 1, the solution to (52) is found as

$$b^* = \frac{1}{\|\overline{C}\|_{\infty}} \mathbb{1}. \tag{53}$$

The solution (53) is applied when $k_j p_j^* < \Delta t_m \ \forall j$.

If $k_j p_j^* < \Delta t_m$ only for some j, in order to derive a less conservative solution, one may adopt a mixed strategy, that consists in applying Theorem 1 for the axes for which this is feasible. This corresponds to

choosing the reference trajectory (28)-(30) with amplitude

$$\hat{a}_i^* = \min(a_i^*, b_i^*), \tag{54}$$

where a_j^* is provided by Theorem 1, for all axes j for which

$$k_j \hat{p}_j^* = k_j \sqrt{\hat{a}_j^* / \gamma_j} \ge \Delta t_m. \tag{55}$$

For the remaining axes, an oscillating motion of the form shown in Fig. 9, with amplitude b_j^* , is selected. Summarizing, in order to track the reference trajectory outlined in the previous discussion and satisfy the minimum firing time restrictions, the following control logic MS can be used. Let $\xi = \min_i k_i p_i^*$. Then

$$MS(p^{*}, \phi^{*}, a^{*}, b^{*}) : \begin{cases} MS_{\Pi}(p_{j}^{*}, \phi_{j}^{*}) & \text{if } \xi \geq \Delta t_{m} \\ MS_{\Pi}(\hat{a}_{j}^{*}) & \text{if } \xi < \Delta t_{m} \wedge k_{j} \hat{p}_{j}^{*} \geq \Delta t_{m} \\ MS_{0}(b_{j}^{*}) & \text{if } \xi < \Delta t_{m} \wedge k_{j} \hat{p}_{j}^{*} < \Delta t_{m}, \end{cases}$$
(56)

where \hat{a}_j^* and \hat{p}_j^* are given by (54) and (55), respectively. In other words, the MS_{II} scheme is applied to track the trajectory provided by Theorem 2 only when the resulting firing time is feasible for all actuators (i.e. $\xi \geq \Delta t_m$), otherwise the mixed strategy MS_0/MS_I is resorted to.

C. Adaptive control scheme for time-varying disturbances

In the following, the case in which the disturbance acting on system (17) is a time-varying signal k(t) is considered. This is of practical interest, whenever the disturbance torque is generated by environmental perturbations. Since the time constants of such perturbations are in the order of the orbital period, they turn out to be usually much larger than the period of the attitude error oscillations. Therefore, one can assume that the variation of k(t) is small during one period of the error oscillations. Under this assumption, it is shown hereafter how the control schemes introduced in Section IV-A can be adapted to cope with time-varying disturbances.

The control law MS_I in (43) can be readily modified as

$$MS_{I}(a^{*}(t)): u(t) = \begin{cases} -1 \text{ if } s(x, \dot{x}; k(t)) \ge a^{*}(t) \\ 0 \text{ if } s(x, \dot{x}; k(t)) \le -a^{*}(t) \\ u_{p} \text{ otherwise,} \end{cases}$$
(57)

where $a^*(t)$ is computed according to (37). Notice that now also Γ in (37) is time-varying, as it depends on k(t).

The adaptation of the control scheme MS_{II} in (45) requires a more careful treatment. First, one has to evaluate (40)-(41) online. In order to make the procedure computationally feasible, this is done only at time instants t_r , such that

$$t_{r+1} = t_r + \Delta t_a, \tag{58}$$

where $t_0 = 0$, and Δt_a is a fixed adaptation step. Then, the control law $MS_{II}(p^*(t), \phi^*(t))$ is applied, with the piecewise constant time-varying parameters

$$p^{*}(t) = p^{*}(t_{r}),$$

$$\phi^{*}(t) = \phi^{*}(t_{r}),$$
for $t_{r} \le t < t_{r+1}$
(59)

where $p^*(t_r)$ and $\phi^*(t_r)$ are computed according to Theorem 2, with $k=k(t_r)$. This amounts to approximate k(t) with a piecewise constant signal for the computation of the reference period and phase. Clearly, Δt_a is a tuning parameter that allows to trade off the computational burden and the performance of the control scheme. The numerical search algorithm required to evaluate (40)-(41) has to be tweaked to avoid that small variations of k(t) result in abrupt changes in $\phi^*(t)$, due to the presence of multiple local minima in $\max\{\sqrt{\sigma(\phi)},\eta(\phi)\}$. This is done by performing at each time t_r a local search in a neighborhood of the previous solution $\phi^*(t_{r-1})$. Another minor amendment has to be adopted in the computation of the parameters $a^L(t;p^*(t),\phi^*(t))$, $a^U(t;p^*(t),\phi^*(t))$, according to (46)-(51). In fact, in (49) one has to compute both \bar{z}_{l+2} and \hat{z}_{l+2} modulo $p^*(t)$, which is now itself a time-varying signal. In order to reset the modulo operator every time interval of length $p^*(t)$, the timing signal $\zeta(t)$ is introduced, such that

$$\begin{cases} \dot{\zeta} = 1 & \text{for } \operatorname{mod}(\zeta, p^*(t)) \neq 0 \\ \zeta = 0 & \text{for } \operatorname{mod}(\zeta, p^*(t)) = 0 \end{cases}$$

$$\tag{60}$$

and $\zeta(0) = 0$. Then, (50) is replaced by

$$\hat{z}_{l+2} = \zeta(z_l) + \frac{|\dot{x}(z_l)|}{q(z_l)} + \frac{q(z_l)}{2} p^*(z_l) + \frac{\sqrt{2}}{4} \sqrt{p^{*2}(z_l) + \frac{h_{l-1}}{\gamma(z_l)}},\tag{61}$$

where $\zeta(z_l)$ denotes the value of $\zeta(t)$ defined by (60) at the time instant z_l , at which a switching curve of the control law MS_{II} is reached.

Finally, the presence of both time varying disturbances and firing time limitations can be tackled by applying the control scheme MS in (56), with the time varying parameters $p^*(t)$, $\phi^*(t)$ and $a^*(t)$.

V. PRECISION POINTING APPLICATIONS

To assess the performance of the proposed approach, a GEO mission and a LEO mission are numerically simulated. In both cases, the objective is to maintain an Earth-pointing attitude q_{IR} rotating at a constant

angular velocity ω_R , using a set of on-off thrusters. The truth model for the simulation is given by (2)-(4). The disturbance torque τ_d in (4) accounts for the most significant environmental perturbations (gravity gradient, atmospheric drag, magnetic moment, solar radiation pressure) as well as the torques arising from the operation of the orbit control system. White noise is added to the commanded thrust (6) in order to model uncertainty in the actuation system. The standard deviation of the thruster noise is set to 5% of the nominal thrust. An extended Kalman filter processing gyro and star-tracker measurements takes care of estimating the spacecraft attitude, angular rate and the disturbance torque, which are used in the computation of the control law. More details on the considered simulation environment and navigation system can be found in [10].

A. GEO mission

Consider a 2000 kg satellite similar to the Small-GEO platform [31] on a geostationary orbit, with $\omega_R = [0, -7.3 \cdot 10^{-2}, 0]^T$ mrad/s. The size of the spacecraft bus is $2 \times 2 \times 2.5$ m³ and the inertia matrix is $I_M = \text{diag}(1.9, 1.47, 1.55) \cdot 10^3 \text{ kg} \cdot \text{m}^2$. The propulsion system consists of the four orbit control thrusters O1-O4 and the eight attitude control thrusters A1-A6b depicted in Fig. 10. Thrusters A3a-A3b and A6a-A6b are fired in pairs, and hence referred to as thrusters A3 and A6. Moreover, A1-A3 produce opposite torques with respect to A4-A6. Each thruster delivers a thrust equal to 1.5 mN. The resulting thrusting configuration can be modeled as in (6), with

$$B = \begin{bmatrix} -2 & 2 & 0 \\ 2 & 2 & 0 \\ 0 & 0 & 4.2 \end{bmatrix}$$
 mN·m. (62)

During station-keeping maneuvers, a disturbance torque is generated due to misalignment of thrusters O1-O4 with respect to the spacecraft center of mass. Such a torque is usually orders of magnitude larger than that generated by environmental perturbations. Because a station-keeping maneuver requires to fire two orbit control thrusters in sequence, to correct for orbital inclination and longitude errors, the disturbance torque is piecewise constant. In the considered setting, one has $\tau_d = [-1.6, 1.4, -2]^T$ mN·m during the first half of the station-keeping maneuver and $\tau_d = [-0.6, -1.5, 0.7]^T$ mN·m during the second half. The maneuver lasts for 3300 s. In order to maintain the desired Earth-pointing orientation, τ_d must be compensated using thrusters A1-A6. The uncertainty affecting the attitude sensors used by the navigation system is modeled as in [10].

In the following, the proposed control strategy is compared to the MPC scheme developed in [10] for disturbance rejection. The MPC scheme is based on a finite horizon reformulation of the optimal control

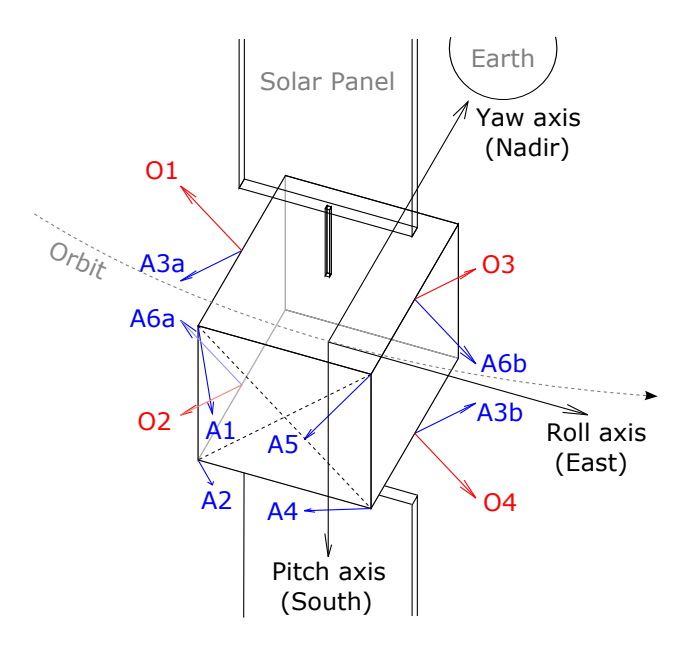


Fig. 10. Thruster configuration: GEO spacecraft.

problem (24) relying on model (9),(11), and requires the solution of a mixed integer linear program (MILP). Such an approach has been found to deliver a significant reduction of both the fuel consumption and the thruster switching frequency with respect to a standard control scheme based on the combination of a linear quadratic regulator and a pulse-width-pulse-frequency modulator.

The required attitude control accuracy is $\|\delta\theta\|_{\infty} < 0.5$ mrad and $\|\delta\dot{\theta}\|_{\infty} < 10~\mu$ rad/s, where $\delta\theta_1$, $\delta\theta_2$ and $\delta\theta_3$ are the roll, pitch and yaw errors, respectively. Then, $W_p = I/(5\cdot 10^{-4})$ and $W_r = I/(10^{-5})$ in (18). According to (62), the control torque on the yaw axis is decoupled from those on the roll and pitch axes. Hence, the results presented in Section III-A can be used for the yaw axis, while those in Section III-B can be applied to the two dimensional system including the roll and pitch axes. This amounts to apply Theorem 2 to system (17) with j=1,2, and Theorem 1 for j=3. Consequently, the control law $\mathrm{MS}_{\mathrm{II}}$ is applied for j=1,2, while MS_{I} is employed for j=3. The resulting control scheme is denoted by $\mathrm{MS}_{\mathrm{II}}+\mathrm{MS}_{\mathrm{I}}$. The period and phase to be tracked are evaluated twice, to account for the impulsive variation of the disturbance at $t=1650~\mathrm{s}$ (due to the switch between two orbit control thrusters). In Fig. 11, the tracking errors $\delta\theta$ and $\delta\dot{\theta}$ obtained with this approach are compared to those resulting from the application of the MPC scheme. The two controllers succeed in keeping the tracking errors within the bounds. Notice that the constraints on the angular rate error are more stringent than the attitude error ones.

The fuel consumption and the switching performance are measured by the sum of the actuator firing

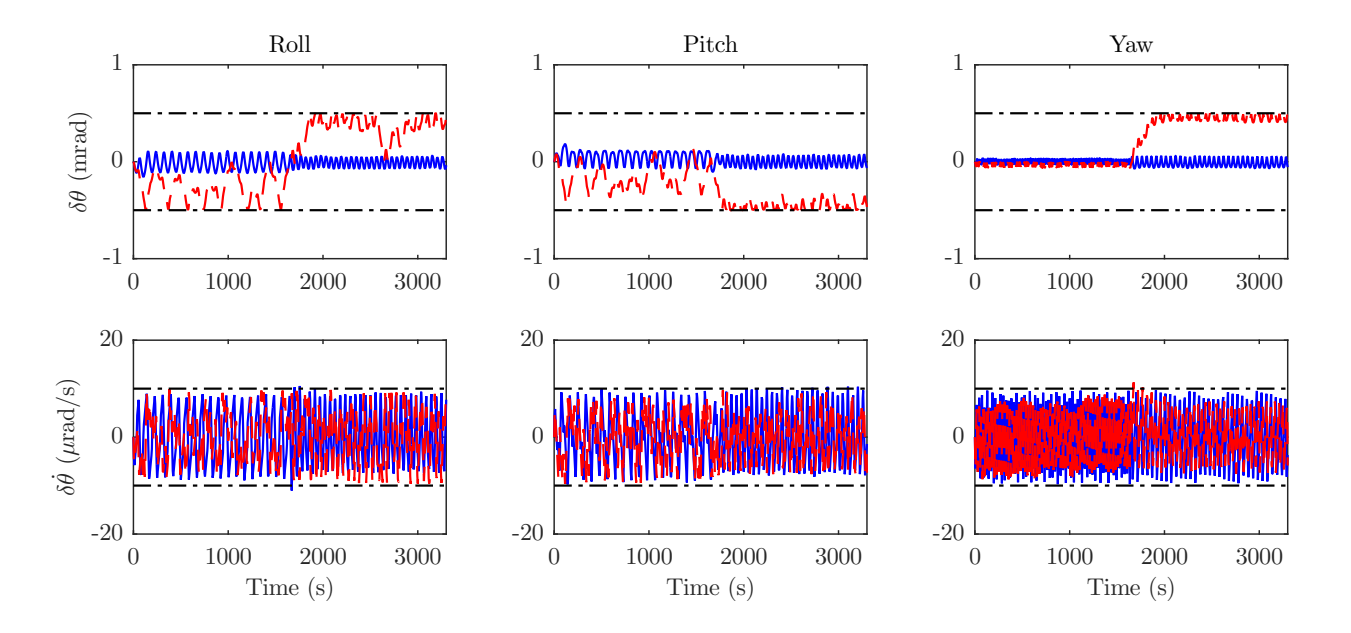


Fig. 11. Tracking errors resulting from the application of the $MS_{\rm II}+MS_{\rm I}$ (blue, solid) and MPC (red, dashed) schemes, with constraints (18) (dash-dotted).

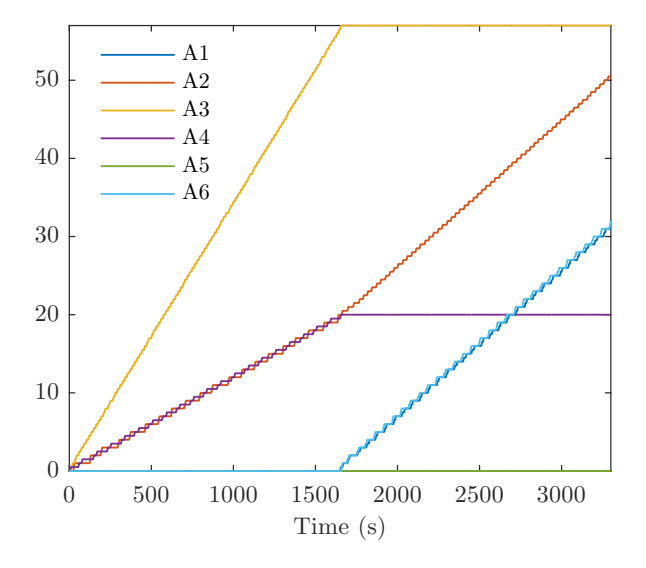


Fig. 12. Time evolution of the number of thruster firings for the $MS_{II} + MS_{I}$ scheme.

times and the maximum number of firings per thruster, respectively. The time evolution of the number of firings required by the $MS_{II} + MS_{I}$ scheme is depicted in Fig. 12, where each line represents a different thruster. Notice that, among the six thrusters A1-A6, only three can be active at the same time to comply with the minimum fuel condition (22). Moreover, those employed during the first part of the maneuver are different from those employed in the second part (except for thruster A2), due to the dependance of

TABLE I

CONTROL SYSTEM PERFORMANCE: GEO MISSION

Parameter	MS _{II} +MS _I	MPC
Firing time (s)	3610	3614
Thruster firings (#)	56	79

the mapping (15) on the direction of the disturbance through the term G^{-1} . The performance of both controllers is reported in Table I. The fuel consumption is approximately the same for the two solutions, but the number of thruster firings commanded by the MPC scheme is 40% higher.

The superior performance of the proposed approach is explained by the fact that the MPC optimization problem has to be solved over a short prediction horizon, in order to retain the computational feasibility of the receding horizon strategy. In this respect, it is worth remarking that the $MS_{II} + MS_{I}$ scheme takes only a fraction of the overall computational time required by the MPC scheme. In fact the time needed to solve the MILP in the MPC scheme is much greater than that required to evaluate Theorem 2 through a one-dimensional search on ϕ_2 . Moreover, while the former has to be done at each sampling instant, the latter is performed only twice per station-keeping maneuver.

B. LEO mission

Consider now a 100 kg minisatellite similar to the BIRD platform [32] on a low Earth orbit, such that $\omega_R = [0, -1.1, 0]^T$ mrad/s. The size of the spacecraft bus is $0.6 \times 0.6 \times 0.6$ m³ and the inertia matrix is $I_M = \text{diag}(6, 5.7, 5.7) \text{ kg} \cdot \text{m}^2$. The propulsion system consists of the six attitude control thruster A1-A6 depicted in Fig. 13. Thrusters A1-A3 produce opposite torques with respect to A4-A6. Each thruster delivers a thrust equal to 0.5 mN. The resulting thrusting configuration can be modeled as in (6), with

$$B = \begin{bmatrix} 0 & 0 & -0.15 \\ -0.15 & 0.15 & 0 \\ 0.15 & 0.15 & -0.15 \end{bmatrix} \text{ mN·m.}$$

$$(63)$$

According to the typical hardware and sensing instruments available onboard this type of minisatellite, the uncertainty of attitude measurements has been set one order of magnitude greater than that considered in the GEO case study. The required pointing accuracy is $\|\delta\theta\|_{\infty} < 0.5$ mrad, corresponding to $W_p = I/(5\cdot 10^{-4})$ and $W_r = 0$ in (18). The matrices C and D resulting in (19) are the same reported in Example 1.

Because the orbit of the spacecraft is uncontrolled, the disturbance torque $\tau_d(t)$, depicted in Fig. 14, is due to environmental sources only. As opposed to the GEO mission example, in this case the disturbance

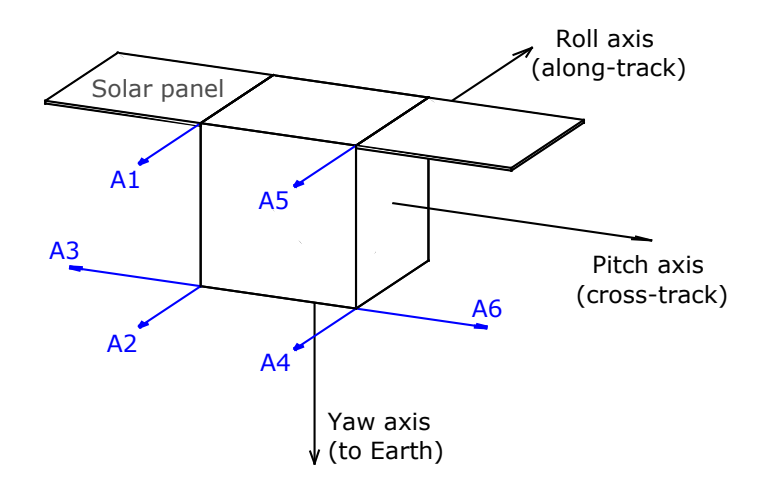


Fig. 13. Thruster configuration: LEO spacecraft.

signal is indeed continuously time-varying, with period equal to the orbital period (5600 s). Moreover, it is such that one or more entries of the vector k(t) in (17) are close to zero at different points along the orbit. These mission characteristics require to account for both disturbance variations and firing duration restrictions, which is accomplished by using the adaptive control scheme $MS(p^*(t), \phi^*(t), a^*(t), b^*)$ in (56). The minimum duration of a thruster firing is set to $\Delta t_m = 0.5$ s, which is compatible with the specification of mN-class engines. An adaptation step $\Delta t_a = 100$ s is employed in (58).

The MS strategy is compared to the MS_0 scheme, which is a common solution for disturbance rejection and attitude regulation with thrusters (see e.g. [33], [34]). The system is simulated for 5600 s. In Fig. 15, it can be seen that the two controllers are able to maintain the tracking error within the required accuracy. Two transitions between the MS_1 and MS_{II} schemes, due to the variation of $k_j(t)p_j^*(t)$ in (56), are clearly visible in the roll error profile between t=1000 s and t=2000 s. Moreover, notice that the tracking error resulting from the application of the MS_0 scheme is kept closer to zero, because the size of the feasible set $x_j \leq b_j^*$ used by this approach is significantly smaller that that adopted by the MS scheme. Clearly, this has an impact on the efficiency of the control system. The performance the control schemes is reported in Table II. The results obtained for the case in which the control law MS_{II} is replaced by MS_1 in (56) are also included for completeness, and denoted by MS/MS_1 . The overall firing time and the maximum number of firings per thruster required by the MS scheme are much lower than the ones delivered by the MS_0 scheme (by 25% and 60%, respectively), resulting in important fuel and electrical power savings, as well as an increased lifetime of the actuators. Moreover, it is confirmed that the use of the MS_{II} control law in the MS scheme provides a significant reduction of the number of switching, with respect to employing only MS_1 .

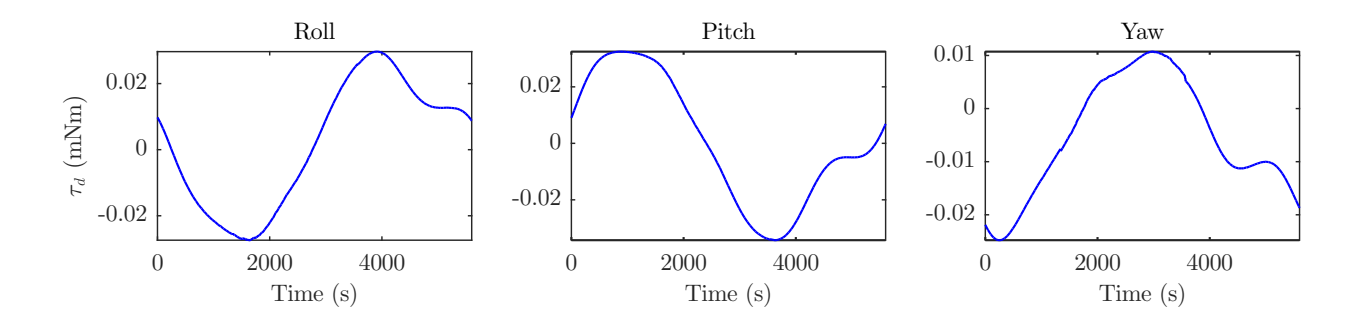


Fig. 14. Profile of the disturbance torque τ_d .

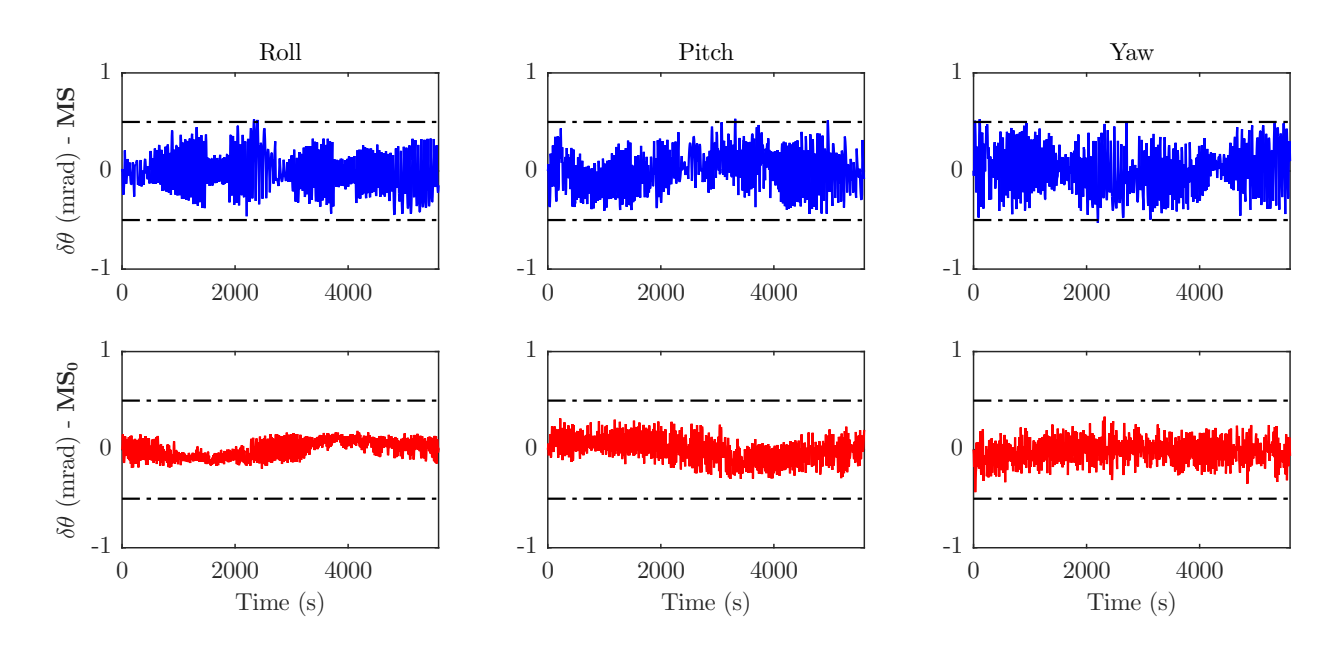


Fig. 15. Tracking errors resulting from the application of the MS and MS₀ schemes, with constraints (18) (dash-dotted).

TABLE II

CONTROL SYSTEM PERFORMANCE: LEO MISSION

Parameter	MS	MS/MS _I	MS_0
Firing time (s)	1730	1726	2310
Thruster firings (#)	78	98	185

Finally, it should be stressed that this last case study is a very challenging test for the proposed control technique, because LEO satellites feature a high orbital rate, which translates into a high variation rate of the environmental disturbance torque. Nevertheless, the controller bandwidth has proven to be sufficient to reject such perturbation, while satisfying the pointing accuracy requirements. Moreover, the required

computational burden is compatible with the limited processing power of spacecraft hardware. In fact, Theorem 2 is evaluated only once every 100 s, through a two-dimensional search on ϕ_1 and ϕ_2 that takes about 20 ms on a 2 Ghz single-core CPU.

VI. CONCLUSIONS

This paper has presented an optimal attitude control scheme for spacecraft precision pointing with on/off actuators. The problem of minimizing the fuel consumption and the thruster switching frequency has been addressed by approximating the attitude error dynamics with a systems of three coupled double integrators subject to a constant disturbance. The online solution to this problem has been exploited in the design of an adaptive control strategy able to deal with both firing duration restrictions and disturbance variations. Simulation results on two realistic missions have shown that the controller is able to keep the pointing error and its derivative within a predefined accuracy, incurring only a minor performance degradation in the presence of time-varying disturbances. The proposed technique represents an attractive option for a number of future small satellite missions, in view of the extremely limited computational burden required. Moreover, this approach can be effective also in different application domains, involving perturbed double integrator dynamics. Future work includes a robustness analysis with respect to parametric uncertainty and the extension of this technique to other classes of linear time-invariant systems.

APPENDIX

Proof of Theorem 1

Let $r = \Gamma^{-1}a$. Then, problem (36) can be rewritten as

$$\min_{\beta,r} \beta$$
s.t. $2/\sqrt{r_j} \le \beta$

$$\|Qr\|_{\infty} \le 1$$

$$\|S\sqrt{rI} \, \mathbb{1}\|_{\infty} \le 1$$

$$r_j > 0.$$
(64)

The statement of the theorem is proven if the feasible solution $r^* = \max\{\|Q\|_{\infty}, \|S\|_{\infty}^2\}^{-1}\mathbb{1}$, $\beta^* = 2/\sqrt{r^*}$ is a global minimum for problem (64). Let \hat{r} , $\hat{\beta}$ be a feasible solution of (64). Then, we get

$$\hat{r}_j \ge \frac{4}{\hat{\beta}^2}, \ \sqrt{r_j} \ge \frac{2}{\hat{\beta}} \quad j = 1, 2, 3,$$
 (65)

and, being $Q_{ij} \geq 0$, $S_{ij} \geq 0 \ \forall i, j$, where Q_{ij} and S_{ij} denote the entries of Q and S, one has

$$1 \ge \sum_{j=1}^{3} Q_{ij} \hat{r}_{j} \ge \frac{4}{\hat{\beta}^{2}} \sum_{j=1}^{3} Q_{ij},$$

$$1 \ge \sum_{j=1}^{3} S_{ij} \sqrt{\hat{r}_{j}} \ge \frac{2}{\hat{\beta}} \sum_{j=1}^{3} S_{ij}, \quad i = 1, 2, 3.$$
(66)

It follows that

$$\hat{\beta} \ge 2\sqrt{\max_{i} \sum_{j=1}^{3} Q_{ij}} = 2\sqrt{\|Q\|_{\infty}},$$

$$\hat{\beta} \ge 2\max_{i} \sum_{j=1}^{3} S_{ij} = 2\|S\|_{\infty}$$
(67)

and therefore

$$\hat{\beta} \ge 2 \max\{\sqrt{\|Q\|_{\infty}}, \|S\|_{\infty}\} = \beta^*,$$
(68)

which concludes the proof.

Proof of Theorem 2

By using (28), constraint (31) can be rewritten as

$$p_1^2 \sigma'(\phi) \le 1,$$

$$p_1 \eta'(\phi) \le 1,$$
(69)

where

$$\sigma'(\phi) = \max_{i} \max_{0 \le t \le p_1} |\sum_{j=1}^{3} C_{ij} \gamma_j f(t/p_1 + \phi_j)|,$$

$$\eta'(\phi) = \max_{i} \max_{0 \le t \le p_1} |\sum_{j=1}^{3} D_{ij} \gamma_j \dot{f}(t/p_1 + \phi_j)|.$$
(70)

Notice that $\sigma'(\phi) = \sigma(\phi)$ and $\eta'(\phi) = \eta(\phi)$, with $\sigma(\phi)$ and $\eta(\phi)$ given by (41), because the peak values of the sums of the p_1 -periodic functions $f(t/p_1 + \phi_j)$, $\dot{f}(t/p_1 + \phi_j)$, evaluated over the period, are independent from the period itself. Then, problem (39) can be rewritten as

$$\min_{\tau,\phi} \tau$$
s.t. $\sqrt{\sigma(\phi)} \le \tau$

$$\eta(\phi) \le \tau, \qquad (71)$$

$$0 \le \phi_j < 1, \ j \ge 2$$

$$\phi_1 = 0, \tau > 0,$$

where $\tau = 2/p_1$. The global minimum of Problem (71) is attained at $\tau^* = 2/p_1^*$, with p_1^* given by (40), which concludes the proof.

REFERENCES

- [1] Sen, A. and Ahmed, N., "Fuel savings in the WHECON attitude control system using an asymmetric controller," *IEEE Transactions on Aerospace and Electronic Systems*, Vol. 12, No. 3, 1976, pp. 349–354.
- [2] Powell, D., "Reliability of the station-keeping activator subsystem of a geostationary satellite," *IEEE Transactions on Aerospace and Electronic Systems*, Vol. 13, No. 3, 1977, pp. 255–263.
- [3] Mueller, J., "Thruster options for microspacecraft: a review and evaluation of state-of-the-art and emerging technologies," *Progress in Astronautics and Aeronautics*, Vol. 187, 2000, pp. 45–138.

- [4] Vaccari, L., Altissimo, M., Di Fabrizio, E., De Grandis, F., Manzoni, G., Santoni, F., Graziani, F., Gerardino, A., Perennes, F., and Miotti, P., "Design and prototyping of a micropropulsion system for microsatellites attitude control and orbit correction," *Journal of Vacuum Science & Technology B*, Vol. 20, No. 6, 2002, pp. 2793–2797.
- [5] Canuto, E., "Drag-free and attitude control for the GOCE satellite," Automatica, Vol. 44, No. 7, 2008, pp. 1766–1780.
- [6] Develle, M. and Xu, Y., "Optimal attitude control allocation via the B-spline augmented virtual motion camouflage method," *IEEE Transactions on Aerospace and Electronic Systems*, Vol. 51, No. 3, 2015, pp. 1774–1780.
- [7] Wright, W. and Ferrer, P., "Electric micropropulsion systems," Progress in Aerospace Sciences, Vol. 74, 2015, pp. 48 61.
- [8] Coletti, M., Ciaralli, S., and Gabriel, S. B., "PPT Development for Nanosatellite Applications: Experimental Results," *IEEE Transactions on Plasma Science*, Vol. 43, No. 1, 2015, pp. 218–225.
- [9] Krøvel, T., Dörfler, F., Berger, M., and Rieber, J., "High-precision Spacecraft Attitude and Manoeuvre Control using Electric Propulsion," 60th International Austronautical Congress, Daejeon, Republic of Korea, 2009.
- [10] Leomanni, M., Garulli, A., Giannitrapani, A., and Scortecci, F., "All-Electric spacecraft precision pointing using model predictive control," *Journal of Guidance, Control and Dynamics*, Vol. 38, No. 1, 2015, pp. 161–168.
- [11] Kienitz, K. H., "Attitude stabilization with actuators subject to switching restrictions: an approach via exact relay control methods," *IEEE Transactions on Aerospace and Electronic Systems*, Vol. 42, No. 4, 2006, pp. 1485–1492.
- [12] Brown, T., "In-flight tuning of the Cassini RCS attitude controller," AIAA Guidance, Navigation, and Control Conference, Portland, Oregon, 2011.
- [13] Jeon, S. W. and Jung, S., "Hardware-in-the-loop simulation for the reaction control system using PWM-based limit cycle analysis," *IEEE Transactions on Control Systems Technology*, Vol. 20, No. 2, 2012, pp. 538–545.
- [14] Agrawal, B., Mcclelland, R., and Song, G., "Attitude control of flexible spacecraft using pulse-width pulse-frequency modulated thrusters," *Space Technology*, Vol. 17, No. 1, 1997, pp. 15–34.
- [15] Hegrenæs, Ø., Gravdahl, J., and Tøndel, P., "Spacecraft attitude control using explicit model predictive control," *Automatica*, Vol. 41, No. 12, 2005, pp. 2107–2114.
- [16] Arantes, G., Martins-Filho, L., and Santana, A., "Optimal on-off attitude control for the Brazilian multimission platform satellite," *Mathematical Problems in Engineering*, Vol. 2009, 2009.
- [17] Kienitz, K. H. and Bals, J., "Pulse modulation for attitude control with thrusters subject to switching restrictions," *Aerospace science and technology*, Vol. 9, No. 7, 2005, pp. 635–640.
- [18] Krovel, T., *Optimal tuning of PWPF modulator for attitude control*, Ph.D. thesis, Norwegian University of Science and Technology, 2009.
- [19] Vander Velde, W. E. and He, J., "Design of space structure control systems using on-off thrusters," *Journal of Guidance*, *Control, and Dynamics*, Vol. 6, No. 1, 1983, pp. 53–60.
- [20] Yao, Y., Yang, B., He, F., Qiao, Y., and Cheng, D., "Attitude control of missile via fliess expansion," *IEEE Transactions on Control Systems Technology*, Vol. 16, No. 5, 2008, pp. 959–970.
- [21] Vieira, M., Galvao, R., and Kienitz, K., "Attitude stabilization with actuators subject to switching-time constraints using explicit MPC," *IEEE Aerospace Conference*, 2011.
- [22] Taylor, A. R., "Adaptive attitude control for long-life space vehicles," *Journal of spacecraft and rockets*, Vol. 7, No. 8, 1970, pp. 924–928.
- [23] Dodds, S., "Adaptive, High Precision, Satellite Attitude Control for Microprocessor Implementation," *Automatica*, Vol. 17, No. 4, 1981, pp. 563–573.
- [24] Garulli, A., Giannitrapani, A., and Leomanni, M., "Minimum Switching Limit Cycle Oscillations for Systems of Coupled Double Integrators," *IEEE Conference on Decision and Control*, Los Angeles, California, 2014, pp. 4655 4660.

- [25] Garulli, A., Giannitrapani, A., and Leomanni, M., "Minimum switching control for systems of coupled double integrators," *Automatica*, Vol. 60, 2015, pp. 115–121.
- [26] Pittelkau, M. E., "Rotation Vector in Attitude Estimation," *Journal of Guidance, Control, and Dynamics*, Vol. 26, No. 6, 2003, pp. 855–860.
- [27] Athans, M., "Minimum-fuel feedback control systems: second-order case," *IEEE Transactions on Applications and Industry*, Vol. 82, No. 65, 1963, pp. 8–17.
- [28] Kaplan, M. H., Modern Spacecraft Dynamics and Control, John Wiley and Sons, 1976.
- [29] Athans, M. and Falb, P. L., *Optimal Control: An Introduction to the Theory and its Applications*, Courier Dover Publications, 2006.
- [30] Kubiak, E. and Martin, M., "Minimum impulse limit cycle design to compensate for measurement uncertainties," *Journal of Guidance, Control, and Dynamics*, Vol. 6, No. 6, 1983, pp. 432–435.
- [31] Kutufa, N., "Small GEO Platform Propulsion System Overview," 5th International Spacecraft Propulsion Conference, Heraklion, Greece, 2008.
- [32] Brieβ, K., Bärwald, W., Gerlich, T., Jahn, H., Lura, F., and Studemund, H., "The DLR small satellite mission BIRD," *Acta Astronautica*, Vol. 46, No. 2, 2000, pp. 111–120.
- [33] Kim, J. and Kim, J., "Disturbance accommodating spacecraft attitude control using thruster," *AIAA/AAS Astrodynamics Conference*, 1996, pp. 800–805.
- [34] Lim, T. W., "Thruster attitude control system design and performance for Tactical Satellite 4 maneuvers," *Journal of Guidance, Control, and Dynamics*, Vol. 37, No. 2, 2014, pp. 403–412.



Mirko Leomanni was born in Siena, Italy, in 1983. He received the M.Sc. degree in Information Engineering in 2008, and the Ph.D. in Information Engineering and Science in 2015, both from the University of Siena. Since 2015, he is a research associate in automatic control and robotics at the University of Siena. His research interests include spacecraft dynamics and control, analysis of switching systems, optimization, and autonomous navigation.



Andrea Garulli was born in Bologna, Italy, in 1968. He received the Laurea in Electronic Engineering from the Università di Firenze in 1993, and the Ph.D. in System Engineering from the Università di Bologna in 1997. In 1996 he joined the Università di Siena, where he is currently Professor of Control Systems. Since 2015, he is the director of the Dipartimento di Ingegneria dell'Informazione e Scienze Matematiche. He has been member of the Conference Editorial Board of the IEEE Control Systems Society and Associate Editor of the IEEE Transactions on Automatic Control. He currently serves as

Associate Editor for Automatica. He is author of more than 170 technical publications, co-author of the book "Homogeneous Polynomial Forms for Robustness Analysis of Uncertain Systems" (Springer, 2009) and co-editor of the books "Robustness in Identification and Control" (Springer, 1999), and "Positive Polynomials in Control" (Springer, 2005). His present research interests include system identification, robust estimation and filtering, robust control, mobile robotics, autonomous navigation and aerospace systems.



Antonio Giannitrapani was born in Salerno, Italy, in 1975. He received the Laurea degree in Information Engineering in 2000, and the Ph.D. in Control Systems Engineering in 2004, both from the University of Siena. In 2005 he joined the Dipartimento di Ingegneria dell'Informazione e Scienze Matematiche of the same university, where he is currently Assistant Professor. His research interests include localization and map building for mobile robots, motion coordination of teams of autonomous agents and attitude control systems of satellites.



Francesco Farina was born in Vibo Valentia, Italy in 1991. He received the B.Sc. degree in Electronic and Telecommunication Engineering in 2013 from the University of Florence and the M.Sc. in Management Engineering in 2015 from the University of Siena. Since 2015 he is a Ph.D. Student in Information Engineering and Science at the University of Siena. His research interests include human locomotion models and inertial navigation systems.



Fabrizio Scortecci received a MS in Aerospace Engineering at the Università di Pisa in 1990. Since his graduation he worked as a Researcher and then as a Project Manager in various theoretical and experimental projects related to electric satellite propulsion, aerothermodynamics and spacecraft systems. During the year 2000 he joined AEROSPAZIO Tecnologie s.r.l. working as Senior Scientist and Manager on programs related to on-orbit application of electric propulsion.